



Power Electronic Systems
Laboratory

© 2015 IEEE

IEEE Journal of Emerging and Selected Topics in Power Electronics, Vol. 3, No. 1, pp. 50-64, March 2015

Modeling and η - α -Pareto Optimization of Inductive Power Transfer Coils for Electric Vehicles

R. Bosshard,
J. W. Kolar,
J. Mühlethaler,
I. Stevanovi,
B. Wunsch,
F. Canales

This material is published in order to provide access to research results of the Power Electronic Systems Laboratory / D-ITET / ETH Zurich. Internal or personal use of this material is permitted. However, permission to reprint/republish this material for advertising or promotional purposes or for creating new collective works for resale or redistribution must be obtained from the copyright holder. By choosing to view this document, you agree to all provisions of the copyright laws protecting it.



Eidgenössische Technische Hochschule Zürich
Swiss Federal Institute of Technology Zurich

Modeling and η - α -Pareto Optimization of Inductive Power Transfer Coils for Electric Vehicles

Roman Bosshard, *Student Member, IEEE*, Johann Walter Kolar, *Fellow, IEEE*, Jonas Mühlethaler, *Member, IEEE*, Ivica Stevanović, *Senior Member, IEEE*, Bernhard Wunsch, *Member, IEEE*, and Francisco Canales, *Member, IEEE*

Abstract—This paper details the optimization of inductive power transfer (IPT) coil systems with respect to efficiency η and area-related power density α as required in electric vehicle applications. Based on analytical calculations and finite-element models, which are discussed and experimentally verified in detail, generally valid design guidelines for high-power IPT systems are derived, and the η - α -Pareto optimization of a scaled 5kW prototype system is presented. Experiments demonstrate a dc-to-dc conversion efficiency of more than 96.5% at a power density of 1.47kW/dm² with coils of 210mm diameter/52mm air gap, including the losses in the resonant capacitors and the power converter. Field measurements validate the predicted stray field with a calculation error of less than 10%.

Index Terms—Electric vehicles, finite-element modeling, inductive power transfer, Pareto optimization.

I. INTRODUCTION

ELECTRIC and hybrid electric vehicles (EV/HEV) have become more and more popular in recent years, in an attempt to reduce the global consumption of fossil fuels. Depending on the form of electricity production, they can have a significantly smaller carbon footprint when compared with traditional vehicles and may at the same time offer a cost advantage due to reduced operating cost. As an alternative to conventional battery charging systems, inductive power transfer (IPT) was recently proposed for the recharging of EV/HEV traction batteries [1]–[5]. Due to the significant simplification of the charging process provided by a contactless system, IPT brings forward the convenience for the users and could, therefore, be a crucial factor for a further increase of the popularity of EV/HEV.

Manuscript received January 28, 2014; revised February 18, 2014; accepted February 24, 2014. Date of publication March 11, 2014; date of current version January 29, 2015. This work was supported by ABB Switzerland Ltd. Recommended for publication by Associate Editor C. T. Rim.

R. Bosshard and J. W. Kolar are with the Power Electronic Systems Laboratory, ETH Zurich, Zurich 8092, Switzerland (e-mail: bosshard@lem.ee.ethz.ch; kolar@lem.ee.ethz.ch).

J. Mühlethaler was with the Power Electronic Systems Laboratory, ETH Zurich, Zurich 8092, Switzerland. He is now with Gecko Simulations, Zurich 8092, Switzerland (e-mail: jonas.muehlethaler@gecko-simulations.com).

I. Stevanović was with ABB Switzerland Ltd., Corporate Research, Baden-Dättwil 5405, Switzerland. He is now with the Federal Department of the Environment, Transport, Energy, and Communications, Biel 2501, Switzerland (e-mail: ivica.stevanovic@bakom.admin.ch).

B. Wunsch and F. Canales are with ABB Switzerland Ltd., Corporate Research, Baden-Dättwil 5405, Switzerland (e-mail: bernhard.wunsch@ch.abb.com; francisco.canales@ch.abb.com).

Color versions of one or more of the figures in this paper are available online at <http://ieeexplore.ieee.org>.

Digital Object Identifier 10.1109/JESTPE.2014.2311302

When designing an IPT system for use in an EV/HEV, a number of constructive boundary conditions must be respected. If no additional mechanical positioning aids for the alignment of the coils are desired, the air gap is given by the construction of the vehicle and the layout of the charging station. The space for the receiver coil on the underfloor of the vehicle and the allowable weight of the components are typically limited, and a high power density of the converter systems and, particularly, a high area-related power density α of the IPT coils is required. In addition, the transmission efficiency η should be as high as possible to simplify the thermal management of the systems. Another design constraint arises from the limitation of the magnetic stray field in the vicinity of the coils. In order to prevent health risks resulting from induced electric fields in human tissue, specifically in the brain and the retina, the stray field is limited by standards [6], [7]. Due to the high power level of EV/HEV battery charging systems, this becomes a challenge in the system design.

The magnetic design of the transmission coils is of key importance in order to satisfy the requirements of a high efficiency and a high power density. Therefore, it is shown in this paper how the two performance indices efficiency η and area-related power density α are related and that a tradeoff is encountered in the optimization of transmission coils for IPT systems, similar to many other power electronic systems [8]. As shown in [9]–[12], a figure-of-merit $FOM = kQ$ given by the product of the magnetic coupling k of the IPT coils and the inductor quality factor Q limits the maximum efficiency of the power transmission to approximately $\eta_{\max} \approx 1 - 2/(kQ)$. Therefore, a high transmission efficiency can be achieved if large coils with a high magnetic coupling are used, which implies a low power density. A higher power density can be achieved if smaller coils are used; however, only a reduced efficiency can be reached even if the quality factor can be increased, e.g., by means of a higher transmission frequency, because of increasing losses in the power electronics and in the core materials that are typically used for flux guidance. This tradeoff is best described by the η - α -Pareto front, which is a physical performance boundary given by the set of designs for which an increase of one of the performance indices η or α results in a decrease of the other. This set of designs is termed the Pareto-optimal designs.

Even though a large number of magnetic structures for IPT coils have been proposed in the literature, no systematic way for optimizing the magnetic design of IPT coils

under consideration of the tradeoff between the transmission efficiency and the area-related power density was presented so far. Therefore, this paper aims to provide a framework for the magnetic optimization of IPT coils, which allows finding the Pareto-optimal designs for a given coil geometry in a systematic manner. Finite-element (FE) models, which are presented in detail and experimentally verified using field and power loss measurements on a 5 kW experimental prototype, are used to derive the η - α -Pareto front for an example coil geometry. The necessary considerations in the selection of a transmission frequency and a resonant compensation topology are highlighted and discussed based on the results of the Pareto optimization.

This paper is structured into six sections. In Section II, general guidelines for the design of series-series and series-parallel compensated IPT systems are presented. Conditions for the design of the transmission coils are derived from analytical design equations. Based on a comparison of different fundamental coil shapes, in Section III, an example geometry is selected for the η - α -Pareto optimization. A winding scheme for circular spiral coils that leads to a high magnetic coupling is presented as a basis for the following sections. The FE models used for the Pareto optimization and the calculation methods for the power loss in the inductor windings and the employed core elements are presented in Section IV. Based on the guidelines derived in Section III and using the FE models from Section IV, an η - α -Pareto optimization for the chosen coil geometry is performed and the tradeoff between the efficiency and the power density is analyzed in Section V. It is shown how a constraint on the magnetic stray field and a thermal model are included in the optimization. From the results, a Pareto-optimal design is selected and an experimental prototype is presented for an output power of 5 kW at a transmission frequency of 100 kHz. The measurement results are presented in Section VI to validate the design process and demonstrate the accuracy of the used FE calculation models. The measured dc-to-dc efficiency of the presented prototype is 96.5% at an area-related power density of 1.47 kW/dm² and 5 kW output power (coil diameter 210 mm/air gap 52 mm). Concluding remarks are given in Section VII.

II. IPT SYSTEM

A block diagram of a typical IPT system operating from the single-phase 230 V/50 Hz grid is shown in Fig. 1(a). An ac-dc converter with power factor correction (PFC) for the grid current is used to produce a controllable dc-link voltage for the IPT system. The IPT system itself consists of an inverter stage at the transmitter side, resonant compensation networks for the transmitter and the receiver coil, and a rectifier circuit at the receiver side. Passive filtering and another dc-dc converter are commonly used to reduce the switching frequency ripple of the charging current and to control the current or the voltage at the interface to the battery.

The specifications of an IPT system typically include the output power P_2 needed for the charging of the battery, the air gap δ across which the output power must be transmitted, and a maximum size for the receiver and the transmitter coil.

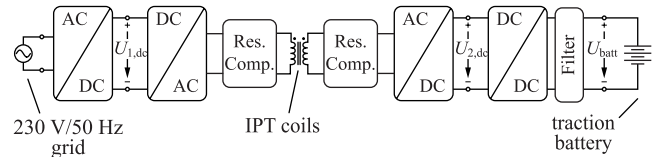


Fig. 1. Block diagram of an IPT system for the charging of the traction battery on an EV/HEV from the 230 V/50 Hz single-phase grid.

TABLE I
SPECIFICATIONS OF THE PROTOTYPE IPT SYSTEM

Var.	Value	Description
P_2	5000 W	output power
δ	52 mm	air gap
$D_{c,max}$	300 mm	max. coil diameter
$U_{1,dc}$	400 V	transmitter-side dc-link voltage
$U_{2,dc}$	350 V	receiver-side dc-link voltage
U_{batt}	350 V	battery voltage

The air gap and the maximum coil size are often given by the geometrical constraints of the application at hand and cannot be changed in the design process. An example specification, which will be used for the design process presented in this paper, is given in Table I. A small-scale IPT system is designed and implemented for an output power of 5 kW and an air gap of 52 mm. For the size constraint, a maximum diameter of 300 mm is assumed for both coils. This constraint is generous considering the air gap of 52 mm, but it will help to highlight the tradeoffs encountered in the selection of a coil size, which will be discussed in detail in Section V, where the prototype system is designed with a coil diameter of 210 mm.

Due to the limited blocking voltages of power semiconductors and the limited current-carrying capability of the components of the employed power electronic converters, also nominal voltages for the dc interfaces of the IPT system at the power supply and the battery are typically included in the specifications. Traction batteries for EV/HEV typically operate at nominal voltages of 300–400 V, hence the IPT system presented in this paper is designed for an output voltage $U_{2,dc}$ of 350 V. As shown in Fig. 1, in a practical application, the input voltage $U_{1,dc}$ is likely provided by a PFC circuit from the single-phase 230 V/50 Hz grid. Therefore, a nominal input voltage of 400 V is specified for the IPT system.

Before proceeding to the magnetic optimization, as a first step in the design of the IPT system, a suitable topology for the resonant compensation networks at the transmitter and the receiver coil must be chosen considering the power and voltage levels and a target switching frequency of the power electronic converters. This will be discussed in the remainder of this section.

A. Possible Resonant Compensation Methods

Due to the inherently large air gap of the IPT system, the magnetic coupling of the IPT coils is low when compared with a traditional transformer. In order to achieve a high

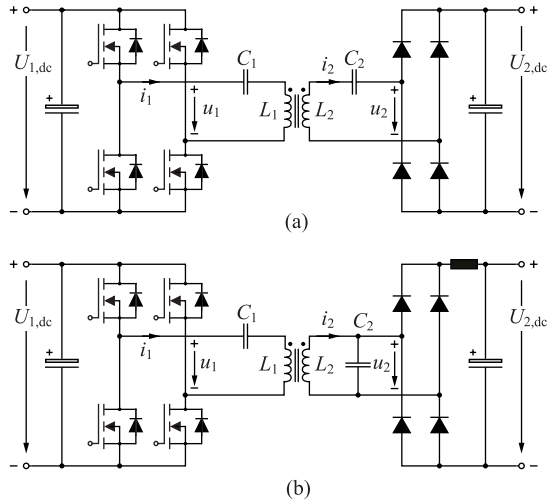


Fig. 2. Equivalent circuit diagrams of a (a) series-series compensated IPT system with a capacitive output filter and (b) series-parallel compensated IPT system with an inductive output filter at the receiver side.

transmission efficiency despite the high leakage inductance, a resonant compensation of the receiver coil L_2 is needed [10]. This is typically implemented with a resonant capacitor C_2 connected either in series or parallel to the receiver coil, as shown in Fig. 2(a) and (b). Note that, depending on the compensation method, also the topology of the output filter at the receiver side is adapted. The resonant frequency f_0 of the receiver-side resonant circuit is an important design parameter, which must be chosen according to the employed type of power semiconductor (MOSFET or Insulated-Gate Bipolar Transistor (IGBT)) and other factors, that will be discussed in detail in Section V. At this point, the resonant frequency is assumed to be a given design parameter.

To reduce the power requirements for the power electronic converter at the transmitter side, another resonant capacitor C_1 is connected to the transmitter coil L_1 . In this way, the phase angle of the input impedance of the resonant circuit as seen by the transmitter-side power converter can be reduced to zero at the resonant frequency, which implies that only active power must be processed by the power converter at this frequency. A parallel compensation of the transmitter coil is also possible, but requires an additional inductor connected in series between the resonant tank and the power converter. This topology is useful for contactless power distribution networks in industrial sites, where a high circulating current is controlled in a track to supply multiple receivers [13]. For a system with only one receiver, as considered in this paper, the power losses in the additional inductor, which must carry the full load current, can be avoided using a series compensation of the transmitter coil.

To decide whether the receiver-side compensation capacitor should be connected in series or parallel to the receiver coil, the geometrical constraints, the power level, and the requirements in terms of a coil misalignment of the targeted application must be considered. To enable a deeper understanding of the involved tradeoffs, in the next section, a mathematical model for both compensation methods is presented with the help of the definitions given in Table II, which are briefly introduced in the following.

TABLE II
DEFINITIONS FOR THE DESCRIPTION OF THE RESONANT CIRCUIT

Definition	Equation
Angular Frequency	$\omega_0 = 2\pi f_0$
Magnetic Coupling	$k = L_h / \sqrt{L_1 L_2}$
Load Matching Factor	$\gamma = R_{L,eq} / (\omega_0 L_2)$
Coil Quality Factor	$Q_i = \omega_0 W_{L_i} / P_{loss,i}$
Inductor Quality Factor	$Q = \sqrt{Q_1 Q_2}$
Total Loss Factor	$\lambda = P_{loss} / P_2$
Efficiency	$\eta = 1 / (1 + \lambda)$

The magnetic coupling k of two magnetically coupled coils is defined by the ratio of the mutual inductance L_h and the geometric mean of the two self-inductances L_1 and L_2

$$k = \frac{L_h}{\sqrt{L_1 L_2}}. \quad (1)$$

Using the definition given in [14], the transmitter and receiver coil quality factors are given as

$$Q_i = 2\pi \frac{W_{L_i}}{P_{loss,i}/f_0} \approx \frac{\omega_0 L_i}{R_i} \quad (2)$$

where $i = 1, 2$ stands for the transmitter the receiver coil, respectively. W_{L_i} is the peak energy stored in the inductor L_i , and $P_{loss,i}$ is the corresponding average power loss. The given approximation is valid under the assumption that the losses in the core material of the IPT coils are small compared with the copper losses and the power loss in the IPT coils can be modeled by parasitic resistances R_i connected in series to the self-inductance of each coil. It will be shown later in this paper that this simplification is valid for the presented prototype design.

Using the analysis given in [15], the load circuit at the receiver side can be modeled as an equivalent load resistance

$$R_{L,eq} = \frac{8}{\pi^2} \frac{U_{2,dc}^2}{P_2} \quad (3)$$

for the converter topology of the series-series compensated IPT system shown in Fig. 2(a). If an inductive output filter is used for the series-parallel compensated IPT system, as shown in Fig. 2(b), the model must be modified to include the current source behavior of the load, which results in

$$R_{L,eq} = \frac{\pi^2}{8} \frac{U_{2,dc}^2}{P_2}. \quad (4)$$

Based on the load model, the load matching factor γ can be defined as

$$\gamma = \frac{R_{L,eq}}{\omega_0 L_2}. \quad (5)$$

In the literature on resonant converters, in addition to the load matching factor, other definitions can be found, such as the loaded quality or the damping. The significance of the load matching factor will become evident hereinafter.

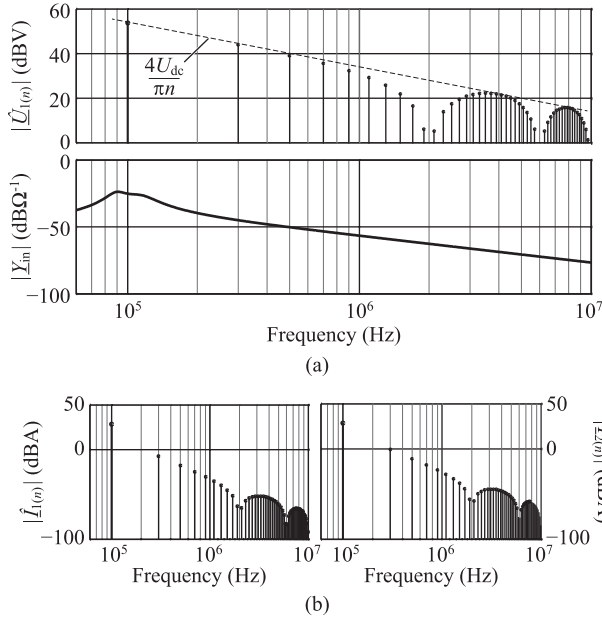


Fig. 3. (a) Spectrum $\hat{U}_{1(n)}$ of the block-shaped voltage at the input of the resonant tank and magnitude of the input admittance \underline{Y}_{in} as a function of the frequency (parasitic capacitances neglected). (b) Spectra of the transmitter coil current $\hat{I}_{1(n)}$ and the receiver coil current $\hat{I}_{2(n)}$. The fundamental components of both currents are more than 30 dBA higher than the first nonzero harmonic component (parameters: prototype system of Section VI).

For the following analysis, it is assumed that the currents in the transmitter and the receiver coils contain only a fundamental component, which is readily validated: for the rectangular output voltage waveform of the inverter bridge legs, the spectrum is calculated as

$$|\hat{U}_{1(n)}| = \frac{4}{\pi} \frac{U_{dc}}{n} \sin(nf_0 t_{on} \pi) \quad (6)$$

for odd harmonic orders n and the ON-time t_{on} of the applied positive or negative voltage pulse. The spectrum of the voltage waveform u_1 is shown in Fig. 3(a). The resulting currents in the IPT coils i_1 and i_2 both depend on the magnitude of the input admittance \underline{Y}_{in} , which is also shown in Fig. 3(a) for the parameters of the prototype system presented in Section VI. From the spectra of the inductor currents, which are shown in Fig. 3(b), it is evident that their fundamental component is more than 30 dBA higher than their first nonzero harmonic component. Consequently, it is sufficient to use the fundamental frequency of the system for the model and neglect all higher harmonic orders.

B. Series-Series Resonant Compensation

In the following, the maximum transmission efficiency η_{max} of the series-series compensated IPT system shown in Fig. 2(a) is calculated. It was shown in [10]–[12] that a series-series compensation with

$$C_1 = \frac{1}{\omega_0^2 L_1} \quad \text{and} \quad C_2 = \frac{1}{\omega_0^2 L_2} \quad (7)$$

leads to the highest efficiency of the power transmission, independently of the magnetic coupling and the load. For this

design, the total loss factor $\lambda = P_{loss}/P_2$ can be calculated as

$$\lambda = \frac{1}{\gamma Q_1 k^2} \left(\gamma + \frac{1}{Q_2} \right)^2 + \frac{1}{\gamma Q_2} \quad (8)$$

which has a minimum at the optimal load matching factor

$$\gamma_{SS,opt} = \frac{1}{Q_2} \sqrt{1 + k^2 Q_1 Q_2}. \quad (9)$$

The maximum transmission efficiency η_{max} of the IPT system at the point where $\gamma = \gamma_{SS,opt}$ is given by

$$\eta_{max} = \frac{k^2 Q^2}{\left(1 + \sqrt{1 + k^2 Q^2}\right)^2} \quad (10)$$

where the inductor quality factor $Q = \sqrt{Q_1 Q_2}$, defined as the geometric mean of the two coil quality factors Q_1 and Q_2 , is introduced for better readability. From (10), it becomes apparent that the maximum efficiency of an IPT system is limited by the product of the magnetic coupling k and the inductor quality factor Q . Therefore, the quantity

$$\text{FOM} = kQ \quad (11)$$

is termed the FOM of IPT systems.

The maximum transmission efficiency η_{max} can only be reached if the load is optimally matched to the receiver inductance according to (9). For equal and large coil quality factors Q_1 and Q_2 , the optimal load matching factor (9) can be approximated by

$$\gamma_{SS,opt} \approx k. \quad (12)$$

Therefore, a design rule for the reactance $\omega_0 L_2$ of the receiver coil follows from the matching condition

$$\omega_0 L_2 = \frac{R_{L,eq}}{\gamma_{SS,opt}} \approx \frac{R_{L,eq}}{k_0} \quad (13)$$

where k_0 is the magnetic coupling of the IPT coils in their nominal position.

At the resonant frequency f_0 , the voltage transfer ratio $|G_{SS,v}|$ is calculated as

$$|G_{SS,v}| = \left| \frac{\hat{U}_2}{\hat{U}_1} \right| = \frac{U_{2,dc}}{U_{1,dc}} = \frac{\gamma}{k} \sqrt{\frac{L_2}{L_1}} \quad (14)$$

and from (12) follows a design rule for the transmitter coil

$$L_1 \approx L_2 \cdot \left(\frac{U_{1,dc}}{U_{2,dc}} \right)^2 \quad (15)$$

to implement a specific voltage transfer ratio.

Note that in order to avoid a phenomenon termed pole splitting or bifurcation in [16]–[18], it is necessary to deviate from the stated design rules by about 15%–25% for the receiver inductance L_2 in a practical design. However, this is not discussed further in this paper, since the provided design considerations apply regardless.

C. Series-Parallel Resonant Compensation

A similar calculation is also possible for the series-parallel compensated IPT system shown in Fig. 2(b). It was shown in [9], [10], and [12] that the same maximum transmission efficiency (10) as for the series-series compensated system can also be achieved in the case of a series-parallel compensation and that the same FOM = kQ is valid. However, in this case, it is also possible to achieve a load-independent voltage transfer ratio

$$|G_{SP,v}| = \left| \frac{\hat{U}_2}{\hat{U}_1} \right| = \frac{\pi^2 U_{2,dc}}{8 U_{1,dc}} = \frac{1}{k_0} \sqrt{\frac{L_2}{L_1}} \quad (16)$$

while a high efficiency and zero phase angle of the input impedance at the resonant frequency can be guaranteed over the whole output power range [19], [20]. An operating point with load-independent voltage gain also exists for the series-series compensated IPT system; however, the phase angle of the input impedance exhibits a high load dependency. This leads to a large amount of circulating reactive power in the resonant circuit and a reduced efficiency in partial-load conditions. In addition, the switched current of the transmitter-side power semiconductors is higher, which depending on the employed semiconductor technology could lead to higher switching losses.

For the design of a series-parallel compensated IPT system with constant-voltage transfer ratio, the resonant capacitors must be chosen as

$$C_1 = \frac{1}{\omega_0^2 L_1 (1 - k_0^2)} \quad \text{and} \quad C_2 = \frac{1}{\omega_0^2 L_2} \quad (17)$$

where k_0 is again the magnetic coupling of the coils in their nominal position. The optimal matching factor that leads to the highest efficiency is

$$\gamma_{SP,opt} = \sqrt{\frac{1 + k_0^2 Q_1 Q_2 + Q_2^2}{1 + k_0^2 Q_1 Q_2}} \quad (18)$$

which for equal and large coil quality factors Q_1 and Q_2 can be approximated by

$$\gamma_{SP,opt} \approx \frac{1}{k_0} \sqrt{1 + k_0^2}. \quad (19)$$

A design rule for the reactance $\omega_0 L_2$ of the receiver coil of a series-parallel compensated IPT system follows as

$$\omega_0 L_2 = R_{L,eq} \frac{k_0}{\sqrt{1 + k_0^2}} \quad (20)$$

and the design rule for the transmitter coil is

$$L_1 \approx L_2 \cdot \left(\frac{8 U_{1,dc}}{\pi^2 k_0 U_{2,dc}} \right)^2. \quad (21)$$

It is clear that due to the coupling dependent selection of the transmitter-side resonant capacitance C_1 according to (17), this design is sensitive to coil misalignment. If the IPT coils are misaligned, the transmitter-side power converter must process reactive power and the efficiency of the power transfer will be reduced due to additional conduction losses and increased losses in the power electronics. However, if a coil

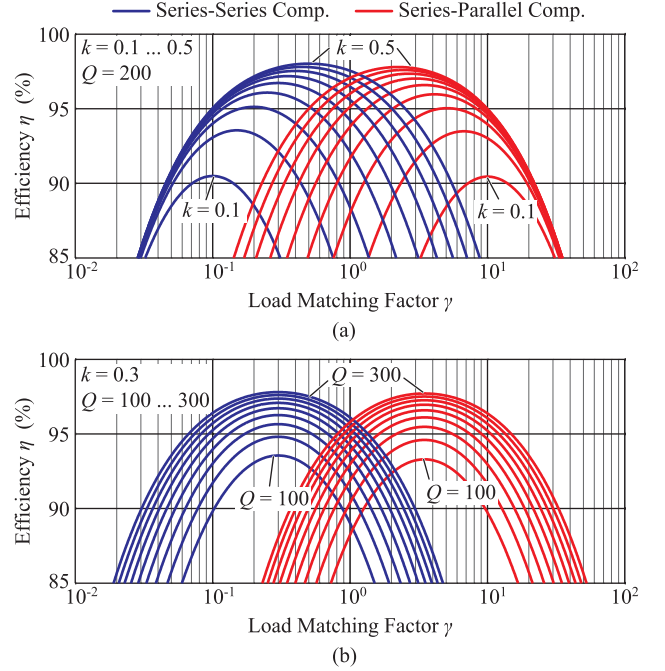


Fig. 4. Comparison of the efficiency η for a series-series compensated IPT system and a series-parallel compensated IPT system as a function of the load matching factor γ and the parameters (a) magnetic coupling ($k=0.1, \dots, 0.5$, steps of 0.05) and (b) inductor quality factor ($Q=100, \dots, 300$, steps of 25).

misalignment is not possible due to the layout of the system, e.g., for the IPT coils of a contactless gate drive supply, this is a favorable solution because it is insensitive to load variations and does not inherently require a communication link between the receiver and the transmitter.

D. Selection of a Compensation Method

Based on the mathematical derivations above, a criterion for the selection of a compensation method can be found. A comparison of the optimal load matching factor for the series-series compensation (12) and the series-parallel compensation (19) shows that the value is significantly higher in the latter case. This implies that for a given load and the same magnetic coupling, the series-series compensation method requires a higher receiver coil reactance $\omega_0 L_2$ than the series-parallel compensation method. Accordingly, if the two IPT systems are designed for the same resonant frequency, the series-parallel compensation method requires a smaller receiver coil self-inductance than the series-series compensation method. As an illustration, Fig. 4 shows a comparison of the achieved efficiency as a function of the load matching factor for different values of the magnetic coupling k and inductor quality factor Q . The required component values for the two compensation methods for the specifications considered in this paper are shown in Fig. 5 as a function of the transmission frequency.

At higher power levels, the size of the coils must typically be increased to obtain the surface area required for sufficient cooling. With the coil size, also the realizable inductance increases. Therefore, for a high-power IPT system, a series compensation topology is preferable, because the low inductance required of the receiver coil in the parallel case

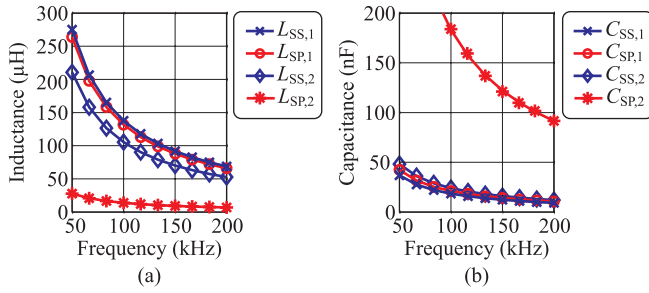


Fig. 5. Required (a) inductance and (b) capacitance values for the series-series (SS) and the series-parallel (SP) compensation method as a function of the transmission frequency according to the derived design rules and the specifications of Table I.

is hardly realizable and a reduction of the frequency is undesirable in many applications, e.g., because of the human (and animal) hearing range. At a low power level, a parallel compensation of the receiver coil is possible if smaller coils are used. It should particularly be considered for a minimization of the receiver coil size, e.g., in biomedical applications, or any application where a constant voltage transfer ratio without the necessity for feedback control is desired.

The series-series compensation method has a number of other advantages. As shown in (7), the compensation capacitances are selected independently of the magnetic coupling or the load. Consequently, the system exhibits a low sensitivity to coil misalignment, and the resonant frequency of the resonant circuit is constant if no component tolerances are present in the system. In addition, since a capacitive filter may be used at the output, the additional filter inductor needed for the series-parallel compensation method can be omitted. This reduces the losses and the volume of the receiver-side power electronics. At the same time, it leads to zero-current switching of the rectifier diodes on the receiver side, which reduces switching losses due to reverse recovery, while it also avoids electromagnetic interference that could result from hard switching.

A commonly discussed disadvantage of the series-series compensation method is the load dependency of the voltage transfer ratio, which could complicate the control and reduce the partial-load efficiency of the system. However, a calculation of the transferred power of the IPT system

$$P_2 = \frac{8}{\pi^2} \frac{U_{1,dc} U_{2,dc}}{\omega_0 L_h} \quad (22)$$

shows that if the two dc-link voltages $U_{1,dc}$ and $U_{2,dc}$ are used for the control of the power transfer by means of additional dc-dc converters, as shown in [5], the series-series compensated IPT system features an excellent partial load behavior. An elegant control method is possible because the output power can be reduced by reducing either or both of the dc-link voltages while the IPT system continues to operate at resonance, which guarantees a high transmission efficiency even in partial-load conditions.

The good performance and the simplicity of this solution are believed to outweigh the additional losses of the required dc-dc converters. Moreover, for a system with the complexity

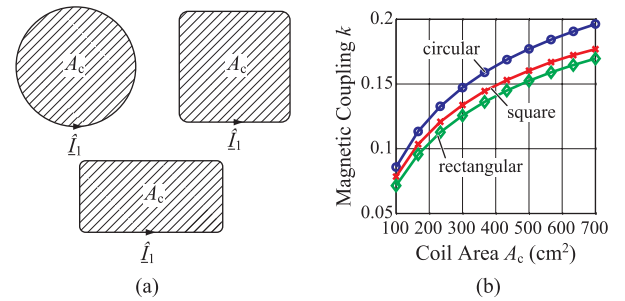


Fig. 6. (a) Schematic drawings of the compared fundamental coil geometries with equal coil area A_c . (b) Comparison of the calculated magnetic coupling k of the fundamental coil geometries as a function of the coil area A_c for an air gap of 52 mm.

of an EV/HEV battery charger, the additionally required communication is considered an acceptable compromise. Given these considerations, for the specifications in Table I, a series-series compensation is found to be most practical and will, therefore, be used for the design of the prototype system.

III. SELECTION OF A COIL GEOMETRY

In the previous analysis, it is shown that the $FOM = kQ$ limits the maximum transmission efficiency of IPT systems, independently of the compensation method. Hence, an optimization of the IPT coil geometry with respect to the two parameters, magnetic coupling k and inductor quality factor Q , is the next step.

For coil designs that include core materials or that have unconventional geometric shapes, FE tools are required for the optimization as analytical calculations are hardly possible. These tools allow calculating equivalent circuit parameters of the coil, predicting the electromagnetic losses in the used materials, dimensioning of the core to avoid saturation, as well as calculation of the stray fields. However, as a starting point for an FE-based efficiency and power density optimization, a fundamental coil geometry and guidelines on how to scale this coil geometry are needed. Therefore, a general understanding of the fundamental relations that contribute to the FOM is provided in this section.

A. Optimization of the Magnetic Coupling k

Typical shapes of IPT inductors include circular, square, and rectangular structures [Fig. 6(a)]. In order to compare the magnetic coupling obtained from the different coil shapes, a 3-D FE tool was used to construct models of a circular, a square, and a rectangular coil geometry in different sizes. For all models, a conductor diameter of 1 mm is used and the number of turns is set to one, i.e., the winding is concentrated at the outer edge of the coil. The air gap is 52 mm, and the rectangular coil is designed with a width to length ratio of 1:2.

The results for the magnetic coupling as a function of the coil area are shown in Fig. 6(b). A circular coil geometry leads to a higher magnetic coupling for a given coil area, which implies a higher transmission efficiency for the same area-related power density of the IPT coil. This can be explained by the distortion of the field distribution around the corners of the

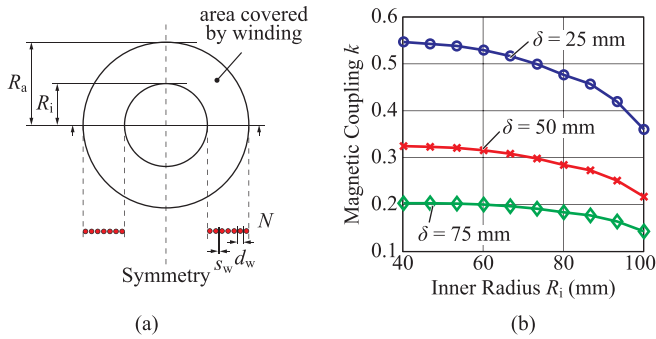


Fig. 7. (a) Schematic drawing of a single-layer spiral coil. (b) Dependency of the magnetic coupling k on the inner radius R_i of two equal spiral coils with a fixed outer radius $R_a = 105$ mm, shown for three different air gaps δ .

square and the rectangular coil shape. However, depending on the aspect ratio of the available space in a practical application, a rectangular coil might be preferable over a circular shape if it would be possible to enclose a significantly larger area.

The next step after the selection of an inductor shape is the design and the placement of the windings on the coil area. Using the analytical models given in [21] for the calculation of circular air coils, an optimal winding scheme is derived in [22]. It is shown that for a single-layer spiral coil made from litz wire and with fixed inner and outer radii [Fig. 7(a)], the way how the area covered by the winding is divided into individual turns has a negligible effect on the magnetic coupling. Furthermore, if high-frequency effects are neglected and extreme or inhomogeneous cases are avoided, the conductor diameter, the separation of the conductors, and the number of turns may be chosen arbitrarily as long as the inner and the outer coil radii are not affected. Therefore, these degrees of freedom can be used for an optimization of the inductor quality factor and to design the self-inductances according to the design rules state above. The inner and the outer radii of a spiral coil are the two parameters that mainly determine the magnetic coupling. For a given outer radius, a smaller inner radius always leads to an improved magnetic coupling; however, as soon as the inner radius is about half of the outer radius, the additional increase of the magnetic coupling becomes small. The calculated result for the magnetic coupling as a function of the inner radius R_i is shown in Fig. 7(b) for $R_a = 105$ mm. A similar result is also presented in [23], where $R_i/R_a = 0.4$ was found as the ratio where no further improvement is observed.

The magnetic coupling can be increased further if a ferrite core structure similar to a pot core is used. This would also allow producing a higher inductance for a given inductor volume, which could potentially lead to an increased power density of the IPT coils. It is expected that a similar analysis including a core would lead to comparable results and, therefore, for this section, no core was considered. However, a core will be included in the FE-based optimization presented in the later sections of this paper.

In addition, only single-layer windings have been considered. This design was chosen as an example, because flat coil designs are preferred for EV/HEV applications to simplify the

mounting of the device, and to keep the self-capacitance of the coil limited and increase the self-resonance far above the intended operating frequency.

B. Optimization of the Inductor Quality Factor Q

The conductor diameter, the separation of the conductors, and the number of turns may be used for an optimization of the inductor quality factor and to design the self-inductances, because these parameters have no significant effect on the magnetic coupling of the spiral coil.

If for a given inner and outer coil radius, more and more windings of a given wire are placed on the coil area and an ever denser winding is produced, the self-inductance of the coil can be increased with approximately $L \propto N^2$ without influence on the magnetic coupling. Since for a constant copper cross section of the litz wire, the winding resistance increases proportionally with the total length $l_w \propto N$ of the conductor, the inductor quality factor increases with approximately $Q \approx \omega_0 L/R_{ac} \propto N$. However, once the separation of the conductors approaches the minimum distance required for the insulation, it is no longer possible to keep the copper cross-sectional constant and the conductor diameter has to be reduced with $d_w \propto 1/N$. Then, the inductor quality factor follows approximately $Q \propto 1/N$, because $R_{ac} \propto l_w/d_w^2 \propto N^3$, due to the reduction of the copper cross section. Therefore, a further increase of the number of turns leads to an efficiency reduction. If a higher number of turns is still needed for the required self-inductance, a different compensation method should be considered or the feasibility of a second layer of windings should be assessed.

These results show that in order to maximize the magnetic coupling of a spiral coil for a given coil area, i.e., the highest area-related power density, a circular coil shape should be chosen. The best winding scheme for a maximization of the FOM is to fill the coil area from the outside toward the center until at least one half of the outer coil radius with closely spaced conductors of a large copper cross section. However, note that a close placement of the windings also increases the parasitic capacitance and lowers the self-resonance frequency of the coils, which imposes an upper limit for the operating frequency.

C. Selection of the Transmission Frequency f_0

The definition of the inductor quality factor $Q \approx \omega_0 L/R_{ac}$ suggests that another method of further increasing its value would be to increase the transmission frequency while adjusting the strand diameter of the copper litz wire to the desired frequency in order to minimize the influence of ac effects. However, an analytical calculation of the total power loss as a function of the transmission frequency is difficult. Therefore, the transmission frequency is included as a degree of freedom in the optimization presented in Section V, where the benefit of a higher transmission frequency is discussed including the power loss in the windings, the core, and the resonant capacitors.

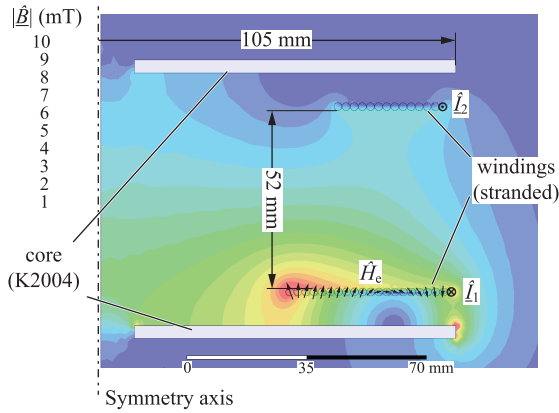


Fig. 8. Visualization of the magnetic flux density of the used FE model. Schematically drawn is the vector of the external magnetic field \hat{H}_e in the transmitter windings (not to scale).

IV. FE MODELING OF IPT COILS

In this section, the theoretical considerations of the previous section are extended with frequency-domain FE models including magnetic components and litz wire that are used for the subsequent η - α -Pareto optimization presented in Section V. The calculations for the loss estimation in magnetic core elements and litz wire are discussed in detail. In addition, details on the employed loss model for the film capacitors used for the resonant compensation are given.

A. Axis-Symmetric FE Models

The coil design that was chosen for the IPT prototype presented in the previous section is axis symmetric. Hence, 2-D FE models are sufficient for the calculation. Fig. 8 shows the simulation model used in the FE tool FEMM¹ and in a commercially available FE software. The litz wire winding is modeled as cylinders of stranded wire with a uniform current density as in the dc case. This prevents the time-intensive calculation of eddy currents in the windings. This approximation is valid because: 1) the litz wire strand diameter is chosen to reduce the high-frequency effects to a minimum; 2) the current distribution inside the windings has only a small influence on the magnetic field on the outside for the investigated geometry; and 3) because in the following, the losses in the windings are calculated using analytical equations together with field values obtained from the FE results and not with the tools provided by the FE method itself. Both of the used FE tools offer this functionality to accelerate their ac-calculation modules.

In order to increase the magnetic coupling of the coils, a ferrite core is added to the coil design. The core is modeled by the relative permeability of the used material K2004 ($\mu_r = 2000$). The conductivity of the core material is low, therefore it is neglected in the FE model ($\sigma < 1$ S/m). All magnetically inactive materials are not modeled, because capacitive effects were excluded from the calculations.

In both tools, the simulated space is bounded by a sphere with a radius that is several times larger than the coil

radius. The sphere radius was determined from a sequence of simulations where the size of the bounding sphere was increased stepwise until no further change in the simulation results could be observed. This process resulted in a sphere radius four times larger than the coil radius. A mixed Dirichlet/Neumann boundary condition on the border of the sphere is chosen to model unbounded open space. In FEMM, this can be achieved by setting up an appropriate mixed boundary condition manually.²

Automatic meshing was used in both cases, which leads to a skin depth based mesh in all materials. To increase the accuracy of the stray field calculation, a maximum mesh size of 5 mm was specified along a radial axis, which has its origin in the center of the air gap. The stray field is then evaluated along this axis for the experimental verification presented in Section VI.

B. Power Loss Calculation

Since the calculation of the power loss in litz wires is not supported by some FE tools, a combination of analytical and FE-assisted calculations is preferred for the loss estimation. The copper loss in the litz wire windings due to the skin effect (including the dc loss) can be calculated analytically by integrating the loss density

$$p_{\text{skin}} = n \cdot R_{\text{dc}} \cdot F_{\text{R}}(f_0) \cdot \left(\frac{\hat{I}}{n}\right)^2 \quad (23)$$

over the total length of the windings. The variable n denotes the number of isolated strands in the litz wire, R_{dc} is the dc resistance per unit length of a single strand of the litz wire, \hat{I} is the current peak value, and $F_{\text{R}}(f_0)$ is a frequency-dependent factor that models the skin effect [24].

The calculation of the loss density due to the proximity effect

$$p_{\text{prox}} = n \cdot R_{\text{dc}} \cdot G_{\text{R}}(f_0) \cdot \left(\hat{H}_e^2 + \frac{\hat{I}^2}{2\pi^2 d_a^2}\right) \quad (24)$$

where d_a is the outer diameter of the litz wire and $G_{\text{R}}(f_0)$ denotes a frequency dependent factor that models the proximity effect [24], however, requires knowledge of the external magnetic field \hat{H}_e penetrating the windings. It is a good assumption that the magnetic field is equal over the total length of one turn of the axisymmetric inductor model. However, the external magnetic field \hat{H}_e differs from turn to turn [Fig. 8]. Therefore, \hat{H}_e must be evaluated in the center of each turn individually in order to calculate the loss density p_{prox} accurately for each turn. The loss density p_{prox} is then multiplied with the length of the individual turn. In a 3-D design, an integration along each turn would be required. The total power loss due to the proximity effect can then be calculated by adding up the power losses of all turns in a coil.

The core loss can be calculated by integrating the core loss density according to the Steinmetz equation

$$p_{\text{core}} = \kappa \cdot f_0^\alpha \cdot \hat{B}^\beta \quad (25)$$

¹Version 4.2, freeware available at www.femm.info (8.1.2014).

²See www.femm.info/Archives/doc/tutorial-magnetic.pdf (8.1.2014).

TABLE III
PARAMETER SPACE FOR THE η - α -PARETO OPTIMIZATION

Var.	Min.	Max.	# Points	Description
D_c	100 mm	300 mm	60	Coil diameter
A_{cu}	1 mm ²	4.7 mm ²	10	Cu cross-section
f_t	50 kHz	200 kHz	5	Target frequency

over the volumes of the two cores. The parameters κ , α , and β are the Steinmetz parameters of the core material ($\kappa = 6.47$, $\alpha = 1.32$, and $\beta = 2$ for the used material).

C. Resonant Capacitors Loss Model

For the resonant compensation of the coils, film capacitors of the B32653 and B32654 series are considered. The capacitors are dimensioned according to their specified maximum rms current and the required capacitance obtained from the calculated IPT coil equivalent circuit models. A safety margin of two with respect to the rated power loss is included to compensate for the reduced heat dissipation due to the arrangement of multiple capacitors in an array.

The power loss in the resonant capacitors is estimated according to

$$P_{cap} = \frac{\tan \delta(f_0)}{\omega_0 C} I_{rms}^2 \quad (26)$$

where $\tan \delta(f)$ is a fit over frequency of the $\tan \delta$ indicated in the datasheets by the manufacturer [25]. The power loss in the resonant capacitors is always included in the results presented in the following.

V. η - α -PARETO OPTIMIZATION

Using the FE models and calculation methods presented in the previous section, in this section, an FE-based optimization of a prototype IPT coil is presented. Based on the optimization results, further insight into the tradeoffs encountered in the design of IPT systems is given.

A. Optimization Methodology

To analyze the physical limits of the chosen coil design, an η - α -Pareto optimization is performed. Considering the specifications of Table I, the coil designs with the diameters and the copper cross sections given in Table III were evaluated in a parameter sweep.

A target frequency f_t was used to select coil geometries from a previously generated lookup table according to the design rules presented in Section II. After an initial magneto-static simulation, the frequency of each design is adapted to the actual mutual inductance L_h of the coils by

$$f'_0 = \frac{1}{2\pi} \frac{8}{\pi^2} \frac{U_{1,dc} U_{2,dc}}{P_2 L_h} \quad (27)$$

which follows from (22). This adjustment ensures that all the specifications of Table I are fulfilled by the simulated design. It can be shown that this adjustment also leads to an optimal matching if the coils fulfill (13) and (15).

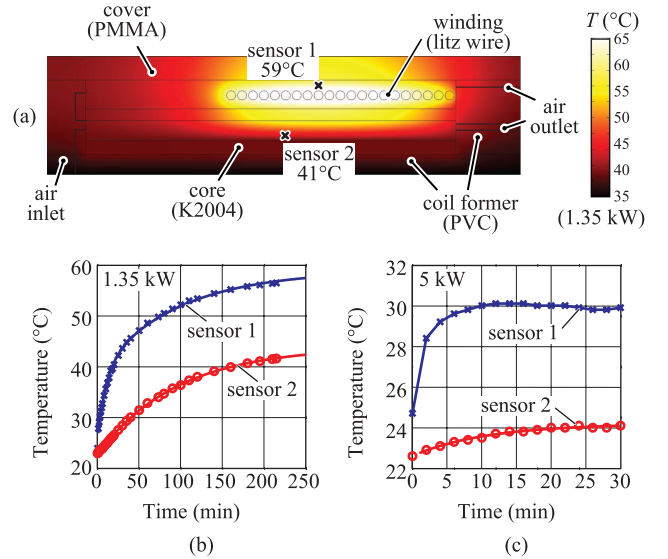


Fig. 9. (a) Thermal simulation model of the presented prototype IPT coil with indicated sensor positions. (b) Temperatures measured with thermocouples at the indicated positions for 1.35 kW output power without cooling. (c) Measured temperatures at 5 kW output power using forced air cooling with compressed air.

Next, the currents in the windings are calculated and the strand diameter of the litz wire is adapted to one-fourth of the skin depth at f'_0 . An FE simulation in the frequency domain is then used to calculate the power losses, as described in Section IV.

B. Thermal Model

A coupled electromagnetic and thermal simulation of the coil designs would be highly time intensive and is therefore hardly possible. In order to still include a simplified thermal model in the optimization, the coil designs that exceed the surface-related power loss density $p_{v,max}$ are removed from the calculated results. Under the assumption of forced air cooling of the coils and a maximum surface temperature 40°C above ambient temperature, $p_{v,max} = 0.2 \text{ W/cm}^2$ is used as an approximation of the thermal limit based on [26]. For a simplified calculation of the copper losses, an average temperature of the winding of 80°C is assumed for all designs.

To ensure the thermal feasibility of the prototype presented in this paper, a thermal simulation of the transmitter coil was made. In Fig. 9(a), the simulation result for an output power of 1.35 kW is shown. To experimentally verify the simulation model, two thermocouples (sensors 1 and 2) were positioned at the locations shown in Fig. 9(a). The measured temperatures shown in Fig. 9(b) are in good agreement with the values obtained from the thermal simulation. During the transmission of the full output power of 5 kW, forced air cooling with compressed air was used. Fig. 9(c) shows the temperature measurement results during the transmission of 5 kW. Due to the active cooling, the steady-state temperatures are reduced significantly. The winding temperature (sensor 1) of 30°C and the core temperature (sensor 2) of 24°C are well below the thermal limit of the employed litz wire (150°C) and the

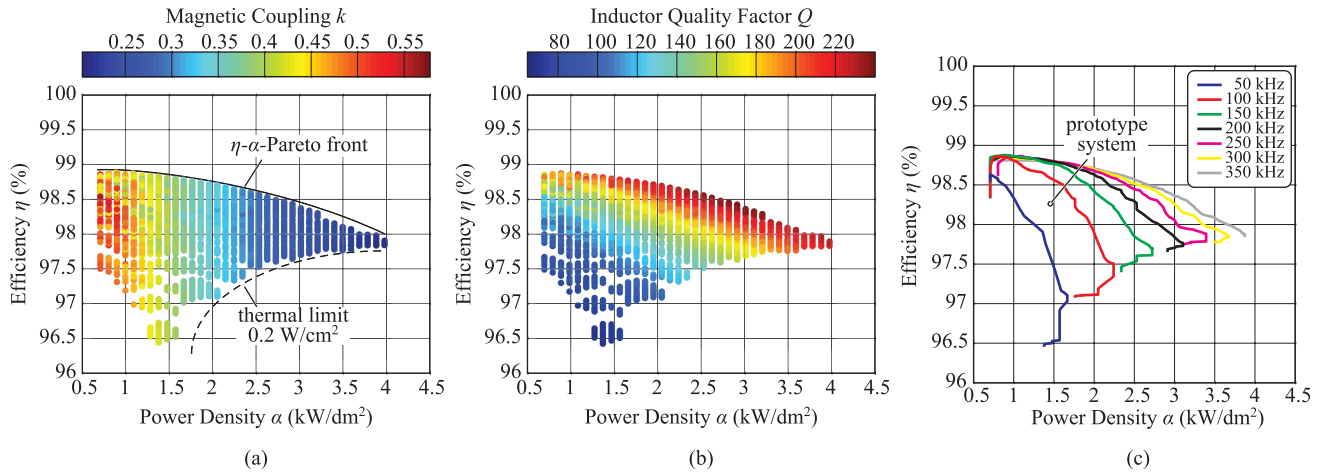


Fig. 10. Results of the η - α -Pareto optimization shown with (a) magnetic coupling k and (b) inductor quality factor Q as parameter. (c) η - α -Pareto fronts for transmission frequencies between 50 and 350kHz. For a given power density, a higher efficiency is possible with a higher transmission frequency if the litz wire strand diameter is adjusted to reduce ac effects.

core material (100°C). The temperature of the used PVC coil former and the PMMA cover are also below their maximum operating temperatures of 60°C and 80°C, respectively.

At 5 kW output power, the surface-related loss density of the presented prototype is approximately $p_v = 0.05 \text{ W/cm}^2$. Given the measured temperature increase of only 8°C above ambient temperature, the assumed thermal limit of $p_{v,\text{max}} = 0.2 \text{ W/cm}^2$ for forced air cooling of the coils seems a valid assumption.

C. Stray Field Constraints

Similar to the thermal constraints of the design, also designs where the stray field exceeds a certain maximum value could be removed from the results of the optimization. Reference values for the stray field are given in [6] and [7]; however, the limits that must be respected strongly depend on the target application. Therefore, no restriction is made for the optimization presented in this paper, but the rms stray field is extracted from the simulation results and discussed below.

D. Discussion of Optimization Results

The calculated performance, including losses in the core, the copper litz wire windings, and the resonant capacitors, of the evaluated design examples is shown in Fig. 10(a) and (b). The η - α -Pareto front that describes the physical tradeoff between the transmission efficiency η and the area-related power density α is clearly visible. The coloring in Fig. 10(a) and (b) corresponds to the calculated magnetic coupling and the inductor quality factor, respectively. As the coil size is decreased, i.e., at an increasing power density, the magnetic coupling is reduced. However, a high efficiency can still be reached if the quality factor can be increased by means of a higher transmission frequency, because this results in a higher $\text{FOM} = kQ$ despite the reduced magnetic coupling. In Fig. 10(c), the Pareto fronts for seven frequencies are outlined. They clearly show that a higher transmission frequency results in a higher transmission efficiency for higher power densities, because of the higher quality factor [Fig. 10(b)].

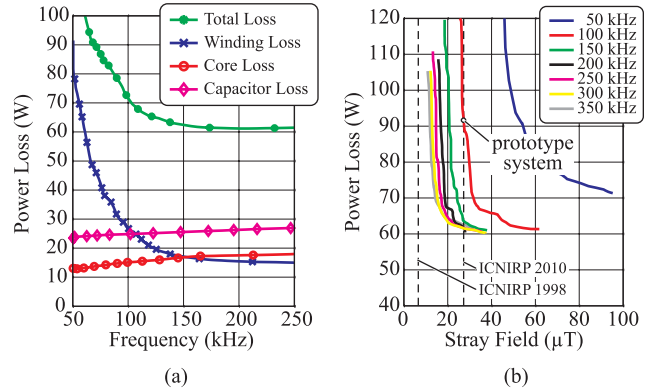


Fig. 11. (a) Power losses of designs with a power density of 1.47 kW/dm^2 (power density of the presented prototype). The winding losses decrease with increasing frequency, whereas the core and capacitor losses increase. However, the reduction of the total losses above 100kHz is small. (b) Power loss as a function of the stray field at a distance of 300 mm from the coil center, shown for transmission frequencies between 50 and 350kHz.

For the design of a prototype system, the power losses of the coil designs with a power density of 1.47 kW/dm^2 were extracted from the optimization results and are shown in Fig. 11(a). It can be observed that the winding losses decrease with increasing transmission frequency. Due to the higher frequency according to the design rules (13) and (15), lower self-inductances can be used, which results in coil designs with fewer turns and lower ac resistances. The losses in the core and the resonant capacitors increase as expected from the Steinmetz equation and the increasing equivalent series resistance at high frequencies described in [25]. As a result, up to about 200 kHz the total losses of the designs decrease. However, the improvement above 100 kHz is small when considering, for instance, the total gate driver losses of the four MOSFETs in the transmitter-side power converter, which double from approximately 1 to 2 W if the switching frequency is increased from 100 to 200 kHz (CMF2012D SiC-MOSFET with 91 nC gate charge and +22/-3 V gate driver voltage). For these reasons, 100 kHz is used as the transmission frequency of the prototype system, which is shown in Fig. 10(c). The selected

design lies approximately 0.3% below the Pareto front for 100 kHz, because of a reduction of the self-inductances by 15% below their optimal value. This adjustment is needed to avoid a pole splitting, which could potentially result in high switching losses due to hard switching of the transmitter-side power semiconductors and controller instability [Section II] [16]–[18].

A number of further tradeoffs and limitations must be considered when selecting a high transmission frequency in a practical design. First, there are technical limitations on how thin the litz wire strands can be manufactured; commercially available copper litz wires reach minimal strand diameters of around 30 μm . At the same time, the filling factor of litz wires decreases with decreasing strand diameter because the required amount of insulation material becomes large with respect to the copper cross section. This leads either to higher copper losses or to a lower power density if the outer diameter of the wire is increased to maintain a constant copper cross section. In addition, with too thin strand diameters, the wires may become fragile and some of the strands might break, which also reduces the effective copper cross section. Moreover, the higher price and limited availability of litz wires with extremely thin strands and large copper cross section must be considered.

As a second limitation, the losses in the power semiconductors of the power electronic converters must be considered. If IGBTs were used as switches, the switching losses due to the stored charge that will occur despite the soft-switching conditions need to be taken into account in a tradeoff analysis [27]–[29]. Also if MOSFETs are used, there are certain frequency-dependent losses in the converter, e.g., the mentioned losses of the gate driver. In addition, the switching speed and required interlock time of the used devices become critical as soon as the switching period reaches the order of magnitude of the time required for turn-ON and turn-OFF of the devices. Moreover, low inductance and capacitance values are needed in the resonant circuit at higher frequencies [Fig. 5], and therefore parasitics in the power electronic converter and the IPT coils become more and more important. For instance, the output capacitance of the switches of the transmitter-side inverter is connected in series to the transmitter-side series resonant capacitor during the ON-state, which alters the effective compensation capacitance. The stray inductance resulting from the converter layout and connection wires to the coils is added to the leakage inductance of the IPT coil system, which results in a reduction of the effective magnetic coupling and, thus, leads to a lower efficiency.

A different tradeoff in the design of IPT coils is shown in Fig. 11(b), where the power loss is shown as a function of the minimum achieved rms stray field observed at a distance of 300 mm from the coil center for seven frequencies. Similar to the η - α -Pareto front, a tradeoff exists for the power loss and the stray field. The stray field at a given observation point can be reduced if smaller IPT coils are used for the power transmission, i.e., the distance of the observation point to the coil windings becomes larger. However, due to the required increase of the power density of the coils, a higher power loss results. As shown in Fig. 10(c), the power loss can be reduced

TABLE IV
SELECTED DESIGN FOR THE PROTOTYPE SYSTEM

Variable	Value	Description
D_c	210 mm	coil diameter
A_{cu}	2.49 mm ²	copper cross-section
f_0	100 kHz	transmission frequency
d_i	71 μm	litz wire strand diameter
α	1.47 kW/dm ²	power density
η	98.25%	transmission efficiency
B_s	26.16 μT	stray field

if the transmission frequency is increased, but the described tradeoff exists nonetheless. With the coil design investigated in this paper, the ICNIRP 2010 standard [6] can only be fulfilled if a transmission frequency above 50 kHz is used and it is not possible to comply with the ICNIRP 1998 standard [7] at the observation distance of 300 mm, even with a frequency as high as 350 kHz. As an alternative solution, passive or active shielding could be included in the coil design to reduce the stray field. Then, also the losses due to eddy currents in the shielding elements must be taken into account, which is possible with the used FE tools. However, since shielding is not needed for the prototype presented in this paper, this is not investigated further.

VI. EXPERIMENTAL VERIFICATION

Taking everything into account, a prototype IPT system was designed for an area-related power density $\alpha \approx 1.47 \text{ kW/dm}^2$ with the parameters listed in Table IV. The system is shown in Fig. 12(a)–(c). A transmission frequency of 100 kHz was used and a strand diameter of 71 μm was chosen for the litz wire based on the skin depth at the selected frequency. From the calculations, a transmission efficiency of 98.25% is expected. The expected stray field of the prototype system is 26.16 μT at a distance of 300 mm from the coil center.

The power converter shown in Fig. 12(a) was constructed for the experimental verification of the used models. Even though for the measurements, a dc-link voltage of 400 V is used, the converter was built with 1.2 kV SiC-MOSFETs ($R_{\text{DS,on}} = 80 \text{ m}\Omega$ at 75°C), which leads to increased conduction losses when compared with a design with 600 V devices. However, the higher blocking voltage will also allow future experiments with higher dc-link voltages, e.g., 800 V supplied from the three-phase grid, and, owing to the low capacitance and high switching speed of the used devices, switching frequencies higher than 100 kHz are also possible. This flexibility of the test setup was preferred over the additional loss reduction that could result from devices with lower rating.

A waveform of the converter output voltage u_1 , the rectifier input voltage u_2 , and the inductor currents i_1 and i_2 at a transmission of 5 kW output power are shown in Fig. 12(d). The close-to-sinusoidal shape of the inductor currents supports the previously presented fundamental frequency model.

In order to assess the quality of the FE models presented in Section IV in terms of calculated power loss, equivalent circuit parameters, and stray field, an extensive experimental

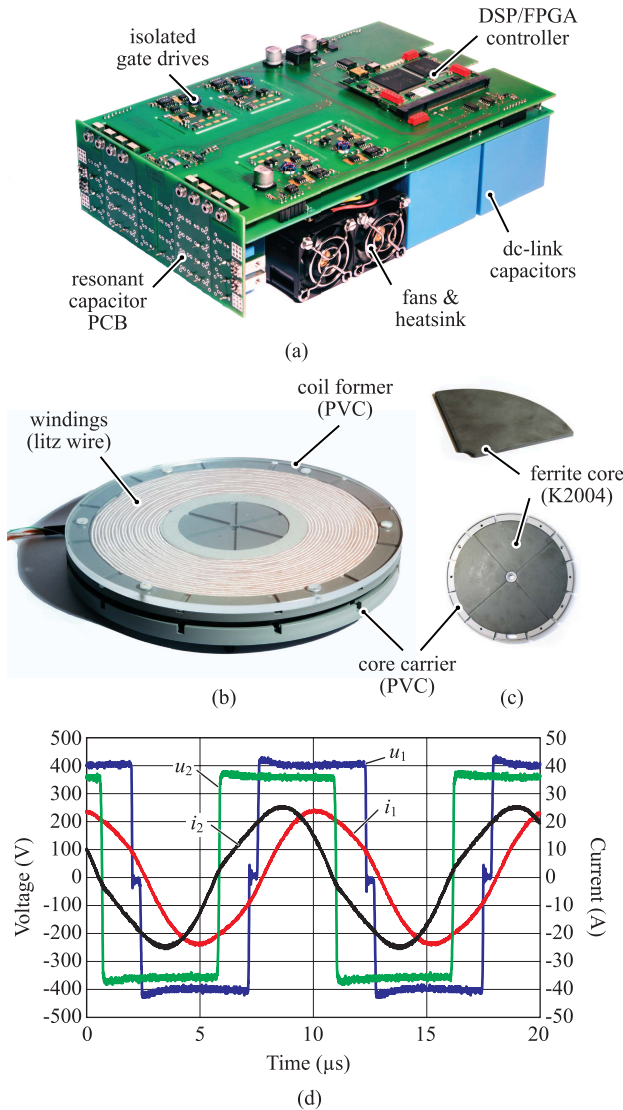


Fig. 12. Prototype IPT system, designed to transmit 5 kW across an air gap of 52 mm at 100 kHz. (a) Test inverter employing SiC MOSFETs. (b) IPT coil with a diameter of 210 mm, windings made from copper litz wire with 630 strands of $71 \mu\text{m}$ diameter. (c) Ferrite core material (K2004) placed in a carrier made from PVC. (d) Waveforms of a measurement at the transmission of 5 kW over an air gap of 52 mm.

verification was performed. In the following, the results of these measurements are compared with the calculated values.

A. Equivalent Circuit Parameters

Table V shows the measured circuit parameters and those obtained from the FE methods. Indicated in brackets is the calculation error relative to the measured values. It can be observed that the self-inductances are calculated accurately by both of the used FE tools. The magnetic coupling is also accurate with an error of less than 10%. The highest error appears for the mutual inductance, because in its calculation according to $L_h = k\sqrt{L_1 L_2}$, the calculation errors in the self-inductances and the magnetic coupling are adding up.

B. Stray Field

To verify the accuracy of the stray field calculation, field measurements were taken with the field probe that was

TABLE V
COMPARISON OF MEASURED AND FE CALCULATED CIRCUIT PARAMETERS (AIR GAP 52 mm)

Var.	Meas.	FEMM	Commerc. FE tool
L_1	122 μH	129.9 μH (+6.5%)	126.8 μH (+3.9%)
L_2	70.3 μH	72.4 μH (+3%)	71.4 μH (+1.6%)
L_h	30.6 μH	33.9 μH (+10.7%)	33.3 μH (+8.8%)
k	0.33	0.35 (+6.1%)	0.35 (+6.1%)

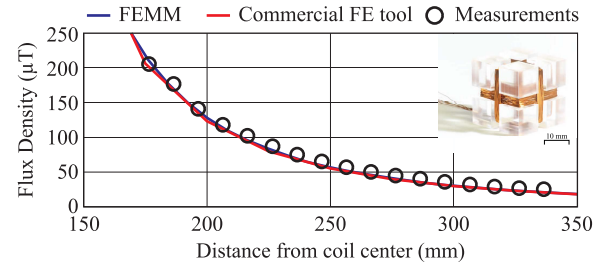


Fig. 13. Comparison of calculated and measured rms stray field of the IPT system. The average absolute value of the relative error with respect to the measurements is 9.3% for FEMM and 11.6% for the commercial FE tool. The design and experimental validation of the field probe is presented in [30].

designed and experimentally tested in [30], along a radial axis with its origin in the center of the air gap. The measurements of the rms stray field are shown in Fig. 13, together with the values calculated by the FE tools and a photograph of the used field probe. If the relative error of the calculation is averaged in absolute value, the tool FEMM shows a deviation of 9.3%. The commercial FE tool deviates by 11.5% from the measured field values.

C. Power Loss

Due to the high frequency of the coil currents and the steep slopes of the switched voltage, it is difficult to reliably measure the power loss in the resonant tank directly. For this reason, only measurements of the dc input power and the dc output power were taken with a power analyzer (WT3000). The used measurement setup is shown in Fig. 14(a). An external load resistor was used to dissipate the transmitted power, while the output voltage was regulated with an electronic load operating in constant voltage mode. In addition, the dc-link capacitor at the output was precharged with a dc supply with a series diode that isolates the supply from the rest of the circuit as soon as the power transmission is initiated.

The power loss measured at the rated output power of 5 kW was then compared to the calculated values of the losses in all components of the prototype system, which are shown in Fig. 14(b). The coil and capacitor losses were calculated as outlined in Section IV. Because of the Zero Voltage Switching operation of the MOSFETs and because an external auxiliary supply is used to power the gate drivers, only conduction losses have to be included for the semiconductor losses of the transmitter-side inverter. In addition, the rectifier diodes (DSEI2x101) on the receiver are soft switched, and therefore only conduction losses have to be calculated for the semiconductor losses of the receiver. A thermal model was used to

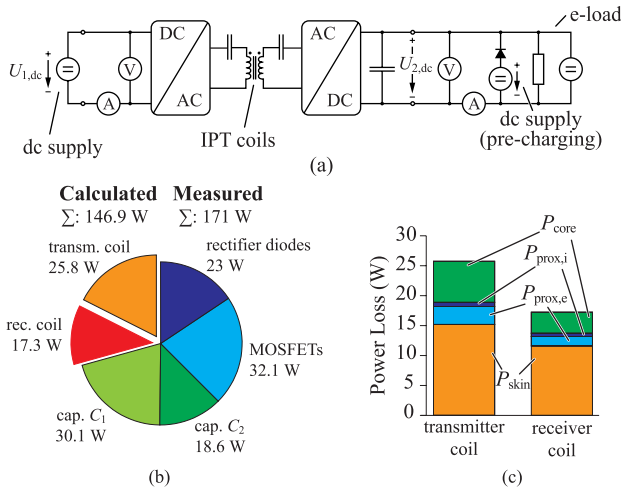


Fig. 14. (a) Schematic diagram of the experimental setup used for the dc-to-dc power loss measurements. (b) Calculated loss components contributing to the total dc-to-dc conversion losses of the prototype IPT system at 5 kW output power and 52 mm air gap. The calculated total loss is 146.9 W, measured were 171 W (−14.2%). (c) FE-calculated loss components in the IPT coils, divided into power loss due to the skin effect P_{skin} (including dc copper loss), the external and internal proximity effect $P_{prox,e}$, $P_{prox,i}$, and core losses P_{core} .

estimate the junction temperature of the devices for the calculation of the conduction losses based on the measured steady-state temperature of 35°C of the custom-made heat sink.

The comparison in Fig. 14(b) shows that the coil losses contribute only about 30% of the total loss, while the remaining loss occurs to approximately equal parts in the resonant capacitors and the semiconductor devices. This clearly illustrates that for a holistic optimization of the IPT system, these components must be considered.

The partitioning of the calculated coil losses into skin effect loss (including dc copper loss), proximity effect loss, and core loss is shown in Fig. 14(c). It can be seen that because of the small strand diameter of the used litz wire (71 μm), the main parts are the dc copper losses. Approximately 24% of the total power loss in the coils result from core losses. The measured steady-state winding temperature with forced air cooling at the maximum power was 30°C and the temperature of the core was 24°C, as discussed in Section V.

The calculated total loss at 5 kW output power is 146.9 W, which means a calculation error of −14.2% with respect to the measured 171 W dc-to-dc power loss. The calculation accuracy of the losses in the resonant capacitors and the semiconductors can be considered high as the calculation is directly based on manufacturer data. All in all, this indicates a good agreement of the FE results with the measurements.

To control the output power, the dc-link voltages at the input and the output were adjusted with the supply and the electronic load shown in Fig. 14(a). As proposed in [5], in a practical realization, this could be implemented with two additional dc–dc converters on both sides of the IPT system. Since the current in the transmission coil can be decreased significantly below its nominal level during partial-load operation, this control method leads to a good performance over a wide operating range, as shown in Fig. 15. The power losses of

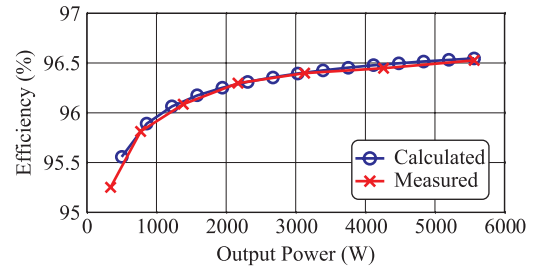


Fig. 15. Calculated and measured dc-to-dc conversion efficiency (including losses in the IPT coils, resonant capacitors, and power semiconductors) as a function of the output power at 52 mm air gap. The output power is adjusted by controlling the dc-link voltage on both sides of the resonant circuit.

the additional dc–dc converters required on both sides of the IPT system are not included in the results shown. However, given the high transmission efficiency that can be reached with this control method, it is expected that the overall conversion efficiency will still be higher than what can be achieved with other methods in partial-load conditions, even if the losses of the required dc–dc converters are included.

The measurements demonstrate a dc-to-dc conversion efficiency of 96.5% of the IPT prototype system at an area-related power density of 1.47 kW/dm² and an efficiency above 95% over a wide operating range, including losses in the IPT coils, the power semiconductors, and the resonant capacitors, which validates the design principles and the optimization process presented in the paper.

VII. CONCLUSION

In this paper, the optimization of a 5 kW IPT system for an air gap of 52 mm under consideration of the tradeoff between transmission efficiency η and the area-related power density α as described by the η - α -Pareto front is presented, and generally valid design guidelines for high-power IPT systems are derived from the results. The used FE models and the power loss calculation are discussed in detail and are experimentally verified. It is shown under which conditions the efficiency of IPT systems can be increased by a higher transmission frequency, which enables a high power density of the IPT system despite the thermal limitations of its components. In the discussion, the encountered tradeoff due to additional losses in the power electronics is highlighted.

From the results of the η - α -Pareto optimization a design is selected for an experimental verification of the design method. Measurements demonstrate the accuracy of the used FE models, including circuit parameters, stray field, and power losses. A dc-to-dc conversion efficiency of 96.5% of the forced air cooled 1.47 kW/dm² IPT prototype system, including the power losses in the IPT coils, the resonant capacitors, and the power semiconductors, for the transmission of 5 kW at 100 kHz is demonstrated by experiments (coil diameter 210 mm and air gap 52 mm).

The work presented in this paper demonstrates the importance of the power electronics in the optimization of IPT systems. Future research could, therefore, address an optimization of the system efficiency under consideration of the losses in all stages of the power conversion, including the coils, the

resonant and dc-link capacitors, the power semiconductors and gate-drivers, and also the power consumption of the cooling system and the control and auxiliary circuits. In addition, for an EV/HEV battery charging system, a wide output power and output voltage range must be taken into account due to the varying state-of-charge of the battery and the desired charging current. Hence, an optimization that takes a certain battery charging profile into account could lead to an improvement of the overall performance of the charging system.

ACKNOWLEDGMENT

The authors would like to thank ABB Switzerland Ltd. for their funding and for their support regarding many aspects of this research project.

REFERENCES

- [1] G. A. Covic and J. T. Boys, "Modern trends in inductive power transfer for transportation applications," *IEEE J. Emerg. Sel. Topics Power Electron.*, vol. 1, no. 1, pp. 28–41, Mar. 2013.
- [2] G. A. Covic and J. T. Boys, "Inductive power transfer," *Proc. IEEE*, vol. 101, no. 6, pp. 1276–1289, Nov. 2013.
- [3] J. Kim *et al.*, "Coil design and shielding methods for a magnetic resonant wireless power transfer system," *Proc. IEEE*, vol. 101, no. 6, pp. 1332–1342, May 2013.
- [4] Bombardier Transportation, Berlin, Germany. (2014, Jan. 10). *Primove—True e-Mobility* [Online]. Available: <http://primove.bombardier.com>
- [5] B. Goeldi, S. Reichert, and J. Tritschler, "Design and dimensioning of a highly efficient 22 kW bidirectional inductive charger for e-mobility," in *Proc. Int. Exhibit. Conf. Power Electronics (PCIM Europe)*, 2013, pp. 1496–1503.
- [6] ICNIRP, "Guidelines for Limiting Exposure to Time-Varying Electric and Magnetic Fields (1 Hz to 100 kHz)," *Health Phys.*, vol. 99, no. 6, pp. 818–836, 2010.
- [7] ICNIRP, "Guidelines for limiting exposure to time-varying electric, magnetic and electromagnetic fields (up to 300 GHz)," *Health Phys.*, vol. 74, no. 4, pp. 494–522, 1998.
- [8] J. W. Kolar, J. Biela, S. Waffler, T. Friedli, and U. Badstübner, "Performance trends and limitations of power electronic systems," in *Proc. 6th Int. CIPS*, 2010, pp. 1–20.
- [9] J. C. Schuder, "Powering an artificial heart: Birth of the inductively coupled-radio frequency system in 1960," *Artif. Organs*, vol. 26, no. 11, pp. 909–915, 2002.
- [10] K. V. Schuylenbergh, *Inductive Powering: Basic Theory and Application*, 1st ed. New York, NY, USA: Springer-Verlag, 2009.
- [11] E. Waffenschmidt and T. Staring, "Limitation of inductive power transfer for consumer applications," in *Proc. 13th Eur. Conf. Power EPE*, 2009, pp. 1–10.
- [12] R. Bosshard, J. Mühlethaler, J. W. Kolar, and I. Stevanović, "The η - α -Pareto front of inductive power transfer coils," in *Proc. 38th IECON*, 2012, pp. 4270–4277.
- [13] A. Green, "10 kHz inductively coupled power transfer—concept and control," in *Proc. 5th Int. Conf. Power Electron. Variable-Speed Drives*, 1994, pp. 694–699.
- [14] R. W. Erickson and D. Maksimovic, *Fundamentals of Power Electronics*, 2nd ed. New York, NY, USA: Springer-Verlag, 2001.
- [15] R. Steigerwald, "A comparison of half-bridge resonant converter topologies," *IEEE Trans. Power Electron.*, vol. 3, no. 2, pp. 174–182, Apr. 1988.
- [16] P. E. K. Donaldson, "Frequency hopping in r.f. energy-transfer links," *Electron. Wirel. World*, vol. 2, pp. 24–26, Aug. 1986.
- [17] C.-S. Wang, G. A. Covic, and O. H. Stielau, "Power transfer capability and bifurcation phenomena of loosely coupled inductive power transfer systems," *IEEE Trans. Ind. Electron.*, vol. 51, no. 1, pp. 148–157, Feb. 2004.
- [18] R. Bosshard, U. Badstübner, J. W. Kolar, and I. Stevanović, "Comparative evaluation of control methods for inductive power transfer," in *Proc. 1st ICRERA*, 2012, pp. 1–6.
- [19] I. Nam, R. Dougal, and E. Santi, "Optimal design method to achieve both good robustness and efficiency in loosely-coupled wireless charging system employing series-parallel resonant tank with asymmetrical magnetic coupler," in *Proc. 5th ECCE*, 2013, pp. 3266–3276.
- [20] W. Zhang, S.-C. Wong, C. K. Tse, and Q. Chen, "Analysis and comparison of secondary series- and parallel-compensated inductive power transfer systems operating for optimal efficiency and load-independent voltage-transfer ratio," *IEEE Trans. Power Electron.*, vol. 29, no. 6, pp. 2979–2990, Jun. 2014.
- [21] S. I. Babic and C. Akyel, "Calculating mutual inductance between circular coils with inclined axes in air," *IEEE Trans. Magn.*, vol. 44, no. 7, pp. 1743–1750, Jul. 2008.
- [22] R. Bosshard, J. Mühlethaler, J. W. Kolar, and I. Stevanović, "Optimized magnetic design for inductive power transfer coils," in *Proc. 28th APEC*, 2013, pp. 1812–1819.
- [23] C. M. Zierhofer and E. S. Hochmair, "Geometric approach for coupling enhancement of magnetically coupled coils," *IEEE Trans. Biomed. Eng.*, vol. 43, no. 7, pp. 708–714, Jul. 1996.
- [24] J. Mühlethaler, "Modeling and multi-objective optimization of inductive power components," Ph.D. dissertation, Swiss Federal Inst. Technol. Zurich, ETHZ, Zürich, The Switzerland, 2012.
- [25] *Film capacitors—Data Handbook*, EPCOS, München, Germany, 2009.
- [26] J. Biela and J. W. Kolar, "Cooling concepts for high power density magnetic devices," in *Proc. PCC*, 2007, pp. 1–8.
- [27] P. Ranstad and H.-P. Nee, "On dynamic effects influencing IGBT losses in soft-switching converters," *IEEE Trans. Power Electron.*, vol. 26, no. 1, pp. 260–271, Jan. 2011.
- [28] G. Ortiz, H. Uemura, D. Bortis, J. W. Kolar, and O. Apeldoorn, "Modeling of soft-switching losses of IGBTs in high-power high-efficiency dual-active-bridge DC/DC converters," *IEEE Trans. Electron Devices*, vol. 60, no. 2, pp. 587–597, Feb. 2013.
- [29] J. Huber, G. Ortiz, F. Krismer, N. Widmer, and J. W. Kolar, " η - ρ -Pareto optimization of bidirectional half-cycle DC/DC converter with fixed voltage transfer ratio," in *Proc. 28th APEC*, vol. 1. 2013, pp. 1413–1420.
- [30] R. Bosshard, J. W. Kolar, and B. Wunsch, "Accurate finite-element modeling and experimental verification of inductive power transfer coil design," in *Proc. 29th APEC*, 2014, pp. 1648–1653.



Roman Bosshard (S'10) received the M.Sc. degree from the Swiss Federal Institute of Technology (ETH) Zurich, Zurich, Switzerland, in 2011, where he is currently working toward the Ph.D. degree with the Power Electronic Systems Laboratory.

He focused on power electronics, ultrahigh-speed electrical drive systems, and control of mechatronic systems, during his studies. His current research interests include inductive power transfer systems, power electronics, and converter design.



Johann Walter Kolar (M'89–SM'04–F'10) received the M.Sc. and Ph.D. (*summa cum laude*) degrees from the Vienna University of Technology, Vienna, Austria.

He is currently a Full Professor of Power Electronics and the Chair of the Power Electronic Systems Laboratory with the Swiss Federal Institute of Technology (ETH) Zurich, Zurich, Switzerland. He has proposed numerous novel PWM converter topologies, and modulation and control concepts, e.g., the VIENNA Rectifier, the SWISS Rectifier, and the Sparse Matrix Converter. In this context, he has authored more than 550 scientific papers in international journals and conference proceedings, two book chapters, and has filed more than 110 patents. He has supervised more than 60 Ph.D. and Post-Doctoral students. He initiated and/or is the founder or co-founder of four ETH spin-off companies. His current research interests include ac–ac and ac–dc converter topologies with low effects on the mains, solid-state transformers for smart microgrid systems, inductive power transfer, ultracompact and ultraefficient SiC or GaN converter modules, power supply on chip systems, multidomain/scale modeling/simulation and multiobjective optimization, and ultrahigh-speed and bearingless motors.

Dr. Kolar is a member of the IEEE, and of Steering Committees and Technical Program Committees of leading international conferences in the field. From 1997 to 2000, he has been serving as an Associate Editor of the IEEE TRANSACTIONS ON INDUSTRIAL ELECTRONICS, and from 2001 to 2013, as an Associate Editor of the IEEE TRANSACTIONS ON POWER ELECTRONICS. He was a recipient of 17 Best Paper Awards of the IEEE Transactions and IEEE Conferences.



Jonas Mühlethaler (S'09–M'12) received the M.Sc. and Ph.D. degrees in electrical engineering from the Swiss Federal Institute of Technology (ETH) Zurich, Zurich, Switzerland, in 2008 and 2012, respectively.

He was involved in modeling and multiobjective optimization of inductive power components during the Ph.D. studies. He is a cofounder of the Gecko-Simulations AG, Zurich, a company that makes simulation tools for power electronics engineers.



Ivica Stevanović (S'03–M'05–SM'12) received the Dipl.Ing. degree in electrical engineering from the University of Belgrade, Belgrade, Serbia, and the Ph.D. degree in electrical engineering from Ecole Polytechnique Fédérale de Lausanne (EPFL), Lausanne, Switzerland, in 2000 and 2005, respectively.

He was a Researcher and Teacher with the California Institute of Technology, Pasadena, CA, USA, in 2000, and at EPFL from 2000 to 2006, before joining the industrial research and development with Freescale Semiconductor, Austin, TX, USA, from

2006 to 2008, as a Senior Research and Development Engineer, and with ABB Corporate Research from 2008 to 2013, as a Principal Scientist. Since 2013, he has been with the Federal Office of Communications, Bienne, Switzerland, where he is currently a Radio Spectrum Specialist representing Switzerland in the international technical bodies for standardization in wireless communications. He has authored more than 70 scientific publications. His current research interests include numerical methods applied to electromagnetic modeling (antennas, waveguides, metamaterial structures, power electronic components, and wireless power transfer) and to statistical and compact modeling of integrated circuits.

Dr. Stevanović was the recipient of the National Science Foundation-Research Experiences for Undergraduates Award from the California Institute of Technology in 2000.



Bernhard Wunsch (M'13) received the International Diploma degree in physics from the Imperial College, London, U.K., and the Diploma degree in physics and the Ph.D. degree in physics for his work in quantum and nanoelectronics from the University of Hamburg, Hamburg, Germany, in 1999, 2002, and 2006, respectively.

He was with a Marie Curie Research Program as a Post-Doctor with Universidad Complutense de Madrid, Madrid, Spain, and the Instituto de Ciencia de Materiales de Madrid, Madrid, on the electronic structure and transport properties of graphene, from 2006 to 2008. From 2008 to 2011, he was a Post-Doctor with Harvard University, Cambridge, MA, USA, on correlated many-particle physics with focus on superconductivity and magnetism. Since 2011, he has been with ABB Corporate Research. His current research interests include modeling and optimization of magnetic components, inductive power transfer, electromagnetic compatibility, and compact models of power electronic components and systems.



Francisco Canales (M'95) received the B.S. degree in mechanical and electrical engineering from Universidad Veracruzana, Veracruz, Mexico, the M.Sc. degree in electronic engineering from Centro Nacional de Investigación y Desarrollo Tecnológico (CENIDET), Cuernavaca, México, and the Ph.D. degree in electrical engineering from the Virginia Polytechnic Institute and State University, Blacksburg, VA, USA.

He was a Senior Research Assistant with the Center for Power Electronics Systems, Virginia Tech, where he was involved in core research and several industry-sponsored projects. He was an Associate Professor with the Department of Electronic Engineering, CENIDET. He is currently a Corporate Research Fellow with ABB Corporate Research Ltd. His current research interests include modular converter designs, resonant switching concepts, and high-efficient conversion topologies for industrial, traction, and renewable energy applications.